Chapter V

ATTENUATION DUE TO THERMAL RELAXATION IN POROUS ROCKS

Thermal relaxation is a well-known mechanism for the absorption of elastic energy in solids. Zener [1948] presents a review of its effects on the anelasticity of metals. Savage [1965] and Armstrong [1979] have treated seismic attenuation due to thermal relaxation in dry granular rocks. A closely related effect is the energy conversion caused by stress-induced phase transitions. Vaisnis [1968] has applied this mechanism to seismic absorption in areas of the mantle containing partial melt.

In this paper we will extend the results of these authors. The frequency dependence will be discussed in greater detail and the magnitude of the loss will be estimated for several cases, such as porous rocks where the pore volume is occupied by gases or liquids, or mixtures of both, with and without phase transitions. Particularly large losses are predicted for rocks containing mixtures of liquid and gas at high pore pressures, water-saturated rocks at high temperatures and rocks containing partial melt. Each of those cases is of interest in the exploration for energy resources.

In the last few years it has been established that pore fluids play a major role in determining seismic velocities [Nur and Simmons, 1969; Domenico, 1976]. It has also been discovered that even minute amounts of volatiles can dramatically increase the absorption in rocks [Pandit and Tozer, 1970; Tittman et al., 1972; Tittman, 1978]. Winkler and Nur [1979] have investigated the effects of a number of variables - including pore and confining pressures, the degree of saturation, and the nature of the pore fluid - on attenuation for both shear and compressional modes of deformation. They found that the introduction of small amounts of gas phases in water-saturated rocks led to a large increase in the attenuation associated with compressional deformations. We will investigate the role of thermal relaxation in these observations.

The magnitude of thermoelastic effects is closely related to the thermal expansivity of the material. The thermal expansivity of gases is typically

about an order of magnitude greater than the thermal expansivity of liquids, which is about an order of magnitude greater than that of solids. Since thermal relaxation is known as a mechanism responsible for significant absorption in metals [Zener, 1948], it would not be surprising to find it playing some role in the absorption in porous fluid or gas-saturated rocks. In contrast to previous investigations of thermal relaxation in rocks, which have considered its effects on dry rocks, we will examine in detail the role of pore fluids.

Physical Principles of the Thermoelastic Effect

It is known from elementary thermodynamics that any material with a nonzero thermal expansivity will be less compressible under adiabatic conditions, when it is thermally isolated, than under isothermal conditions. Adiabatic compression is accompanied by a temperature change, which depends on the thermal and elastic properties of the material. Because for all wavelengths and frequencies of interest in seismology the flow of heat from the peak to the trough of a wave traveling in a homogeneous medium may be neglected [Savage, 1965], wave propagation is controlled by the adiabatic properties of the rock.

In contrast, in a heterogeneous medium such as a porous rock, we can distinguish between two or three kinds of adiabatic responses. When a sudden pressure change is applied to a material with heterogeneous thermoelastic properties, each pore of grain responds adiabatically, producing a spatially heterogeneous temperature change. This results in local heat flow from regions of higher than average stress or greater than average thermal expansivity to regions of lesser stress or expansivity. As the temperature differences relax, some additional strain takes place. The deformation may still be considered adiabatic, now based on the average properties rather than on the local microscopic properties. Furthermore, when more then two phases of the same component, e.g. steam and water, are present, thermal equilibrium is not a sufficient condition for thermodynamic equilibrium, as one of the phases may have become unstable. Equilibrium in response to a pressure increase implies some mass transfer from the less dense phase to the denser phase, accompanied by a release or absorption of the latent heat for the transformation.

We will first derive an exact solution for the mechanical response of an idealized heterogeneous medium, that is, a rock with a random distribution of flat pores of uniform thickness. The result enables us to draw some conclusions about the frequency dependence of the attenuation in rocks with more complicated structures and about the relationships between the magnitude of the absorption and the modulus defect. The modulus defect is defined as the relative change in modulus between the high-frequency unrelaxed and the low-frequency relaxed limits.

An Exact Solution

The process of conversion of wave energy into heat may be described in detail when the geometry of the inhomogeneity is known. For simple geometries this may be done analytically. Here we consider the case of a flat inclusion in an otherwise homogeneous medium. A random distribution of such inclusions will show similar behavior when the inclusions are uncorrelated.

The geometry is illustrated in figure 5.1. Notation and definitions of the parameters we will be using are given in table 5.1. An instantaneous application of a small pressure change P implies a proportional change in temperature $\bar{T}$ by an amount

$$\bar{T} = b\,P \tag{5.1}$$

throughout the rock. If $\bar{T}$ varies in space, flow of heat across finite temperature gradients will take place, with a resulting increase in entropy and an irreversible conversion of mechanical energy into heat. Spatial variations in $\bar{T}$ can result either from inhomogeneities in P or b, or both. In a dry rock with an irregular distribution of pores and cracks, one might expect inhomogeneities in P to dominate since stress concentrations will be present at grain boundaries and the edges of cracks. This case has been considered by Savage [1965]. In fluid-saturated rocks the fluid will support much of the compressional stress in the vicinity of flat cracks. Since the stress heating coefficient b is typically an order of magnitude greater for liquids than solids, we might expect inhomogeneities in b to play a significant role here.

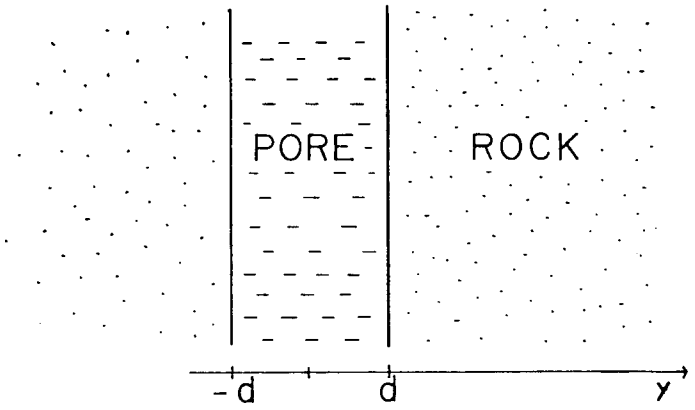

FIG. 5.1. Geometry of rock model used in diffusion solution.

parameter	symbol	definition
isothermal bulk modulus	K	$-V\left(\frac{\partial P}{\partial V}\right)_T$
heat capacity	c	$T\left(\frac{\partial S}{\partial T}\right)_P$
thermal expansivity	α	$\frac{1}{V}\left(\frac{\partial V}{\partial T}\right)_P$
adiabadic bulk modulus	K'	$-V\left(\frac{\partial P}{\partial V}\right)_S$
stress heating	b	$V\left(\frac{\partial T}{\partial P}\right)_S$
diffusivity	D	$\frac{dT}{dt} / \frac{\partial^2 T}{\partial y^2}$
thermal conductivity	h	$D\rho c$

TABLE 5.1. Notation and definitions for thermal parameters.

For the geometry in figure 5.1 both the material properties as well as the strain ϵ and the temperature depend only on y. For flat inclusions the pressure is uniform. The heat flow will thus be described by the one-dimensional diffusion equation, which has the form

$$\frac{dT}{dt} = D \frac{\partial^2 T}{\partial y^2} + b \frac{dP}{dt} \tag{5.2}$$

when the adiabatic heating effect is included. Equation (5.2) may be used to solve for the temperature when the diffusivity D is locally constant. At interfaces, continuity of temperature and heat flow must also be satisfied. Given the temperature, the strain ϵ is obtained from

$$\epsilon = \frac{1}{K} P + \alpha(T-T_o) \tag{5.3}$$

Thus, from a knowledge of the diffusivity, heating coefficient, and thermal expansivity, we can determine the temperature and strain response to any applied stress function, P(t).

When the applied pressure is a sinusoidal function of time

$$P = P_o e^{i\omega t} \tag{5.4}$$

Equation (5.2) becomes

$$i\omega \hat{T} = D \frac{\partial^2 \hat{T}}{\partial y^2} + i\omega b \tag{5.5}$$

where

$$\hat{T} = \frac{T-T_o}{P} \tag{5.6}$$

Similarly, equation (5.3) becomes

$$S(\omega) = \frac{1}{K} + \alpha\hat{T} \tag{5.7}$$

where $S(\omega)$ is a complex, frequency-dependent compliance, ϵ/P. When $S(\omega)$ is known the attenuation parameter Q is obtained from

$$\frac{1}{Q} = \tan \delta = \frac{-Im[S(\omega)]}{Re[S(\omega)]} \tag{5.8}$$

where δ is the phase angle between stress and strain. O'Connell and Budiansky [1978] discuss the relationship between this and various other definitions for Q that have been used in the literature.

A general solution to (5.5) has the form

$$\hat{T} = A_1 \cos h\left[\frac{y}{d}(i\omega\tau_1)^{\frac{1}{2}}\right] + A_2 \exp\left[-\frac{y}{d}(i\omega\tau_2)^{\frac{1}{2}}\right] + b \tag{5.9}$$

where

$$\tau_1 = \frac{d^2}{D_1} \tag{5.10}$$

$$\tau_2 = \frac{d^2}{D_2} \tag{5.11}$$

Symmetry considerations imply that $A_2 = 0$ for $|y| < d$. The condition that T be bounded for large y implies that $A_1 = 0$ for $y > d$. The solution may therefore be written as

$$T = A_1 \cos h\left[\frac{y}{d}(i\omega\tau_1)^{\frac{1}{2}}\right] + b_1 \quad \ldots\ldots \quad |y| < d \tag{5.12}$$

$$T = A_2 \exp\left[-\frac{|y|}{d}(i\omega\tau_2)^{\frac{1}{2}}\right] + b_2 \quad \ldots\ldots \quad |y| > d \tag{5.13}$$

A_1 and A_2 are determined by imposing continuity of temperature and heat flow at the interface. Continuity of temperature implies

$$A_1 \cos h\left[(i\omega\tau_1)^{\frac{1}{2}}\right] A_2 \exp\left[-(i\omega\tau_2)^{\frac{1}{2}}\right] = b_2 - b_1 \qquad (5.14)$$

and continuity of heat flow:

$$\frac{h_1 A_1}{d}(i\omega\tau_1)^{\frac{1}{2}} \sin h\left[(i\omega\tau_1)^{\frac{1}{2}}\right] = -\frac{h_2 A_2}{d}(i\omega\tau_2)^{\frac{1}{2}} \exp\left[-(i\omega\tau_2)^{\frac{1}{2}}\right] \qquad (5.15)$$

where h_1 and h_2 are the thermal conductivities. Solving (5.14) and (5.15) we get:

$$A_1 = \frac{b_2 - b_1}{\cos h\left[(i\omega\tau_1)^{\frac{1}{2}}\right] + \frac{h_1}{h_2}\left(\frac{\tau_1}{\tau_2}\right)^{\frac{1}{2}} \sin h\left[(i\omega\tau_2)^{\frac{1}{2}}\right]} \qquad (5.16)$$

$$A_2 = -A_1 \frac{h_1}{h_2}\left(\frac{\tau_1}{\tau_2}\right)^{\frac{1}{2}} \frac{\sin h\left[(i\omega\tau_1)^{\frac{1}{2}}\right]}{\exp\left[-(i\omega\tau_2)^{\frac{1}{2}}\right]} \qquad (5.17)$$

By subtracting the initial adiabatic strain from the total strain given in Equation (5.7), and integrating over y, we obtain the total displacement, U, per unit of applied pressure caused by the relaxation of temperature differences.

$$U = \frac{2d\left[\alpha_1 - \alpha\frac{h_1\tau_1}{h_2\tau_2}\right](b_2 - b_1)}{(i\omega\tau_1)^{\frac{1}{2}} \cot h\left[(i\omega\tau_1)^{\frac{1}{2}}\right] + r(i\omega\tau_1)^{\frac{1}{2}}} \qquad (5.18)$$

where r is given by

$$r = \frac{h_1}{h_2}\left(\frac{\tau_1}{\tau_2}\right)^{\frac{1}{2}} \qquad (5.19)$$

Equation (5.18) may be rearranged to get

$$U = \frac{-2d}{T\rho_1 c_1} \frac{(b_1 - b_2)^2}{(i\omega\tau_1)^{\frac{1}{2}} \cot h\left[(i\omega\tau_1)^{\frac{1}{2}}\right] + r(i\omega\tau_1)^{\frac{1}{2}}} \qquad (5.20)$$

where use has been made of the relation

$$b = \frac{\alpha T}{\rho c} \tag{5.21}$$

The Taylor-series expansion of the hyperbolic cotangent function implies

$$s \cot h(s) = 1 + \frac{s^2}{3} + \frac{s^4}{45} \quad ..... \tag{5.22}$$

It follows from equations (5.20) and (5.22) that the displacement U ranges from

$$\Delta U = \frac{2d}{T\rho_1 c_1} (b_1 - b_2)^2 \tag{5.23}$$

to zero as frequency goes from zero to infinity, and that the imaginary component vanishes at both limits.

From our definition for Q, equation (5.8), it follows that when

$$\Delta U << U_o \tag{5.24}$$

where U_o is the initial displacement, the attenuation is approximately given by

$$\frac{1}{Q} = \frac{ImU(\omega)}{U_o} \tag{5.25}$$

The ratio

$$\frac{\Delta M}{M} = - \frac{\Delta U}{U_o} \tag{5.26}$$

is often referred to as the modulus defect. It follows from (5.8) that the attenuation, as a function of frequency, may be obtained by multiplying the imaginary part of the inverse of the denominator in equation (5.20) by the modulus defect.

Frequency dependence. Figure 5.2 shows the normalized attenuation $M/Q\Delta M$, as a function of frequency, for three different values of r. One may approximate the response of a more complicated rock by adding the creep due to each crack thickness; a result for three different crack thicknesses is shown in figure 5.3.

Inspection of equations (5.20), (5.22) and (5.25) shows that the attenuation is proportional to the square root of frequency at frequencies much less than $1/\tau_1$ and is inversely proportional to the square root of frequency at high frequencies. Most previous work on linear attenuation mechanisms in rocks [Vaisnis, 1968; Savage, 1966; White, 1975; Dutta and Ode, 1979] has assumed that diffusion-controlled mechanisms could be treated as either a single exponential decay (relaxation time), or a limited distribution of relaxation times, referred to as absorption bands [Kanamori and Anderson, 1977; Minster, 1978]. Figure 5.4 shows the curve from figure 5.2 for $r = 1$. For comparison a plot of the attenuation due to a single relaxation of the standard linear solid [Zener, 1948] is also shown. The comparison shows clearly that the attenuation for this idealized rock model is spread out over a much wider range of frequencies than is the attenuation due to a single relaxation time, and the maximum attenuation is just about half the attenuation for the standard linear solid model. The diffusion solution has the attenuation decreasing with square root of frequency, $\omega^{\frac{1}{2}}$, away from the peak, while the standard linear solid goes as frequency to the first power, ω. Strictly speaking, it can therefore be concluded that an infinite distribution of standard linear solid elements would be required in order to describe the loss caused by any mechanism controlled by diffusion, even in a rock where all the inhomogeneities are of the same size and shape. An actual rock will of course contain a wide range of sizes and shapes; consequently an even broader range of relaxation times would be required to describe its mechanical response.

Thermal parameters for different materials of interest in seismology are listed in table 5.2. All of the materials listed have diffusivities of the order of 1 mm^2/s; this implies that inhomogeneities with dimensions on the order of one millimeter will contribute most to the absorption of seismic waves. As the characteristic time constants, τ_1 and τ_2, are proportional to the crack thickness squared, a relatively narrow distribution of pore sizes will cause loss over a wide range of frequencies.

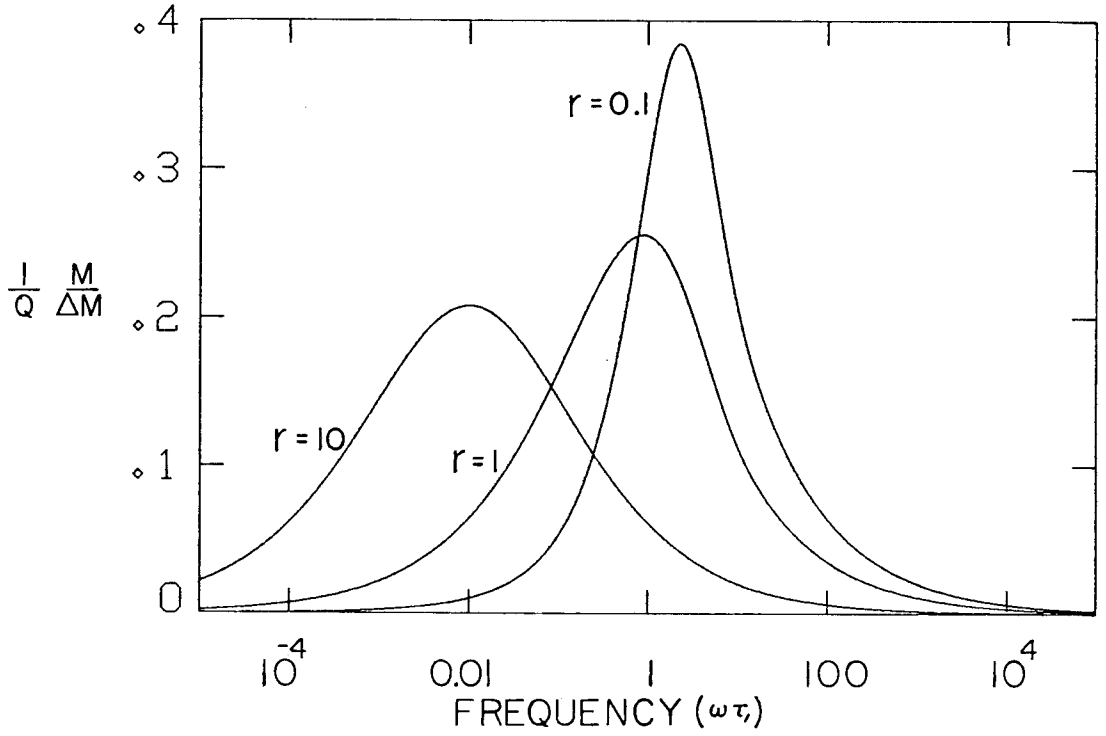

FIG. 5.2. Normalized attenuation $M/Q\Delta M$, as a function of normalized frequency $\omega\tau_1$. Curves for three different values of the thermal-impedance ratio r (5.19) are shown.

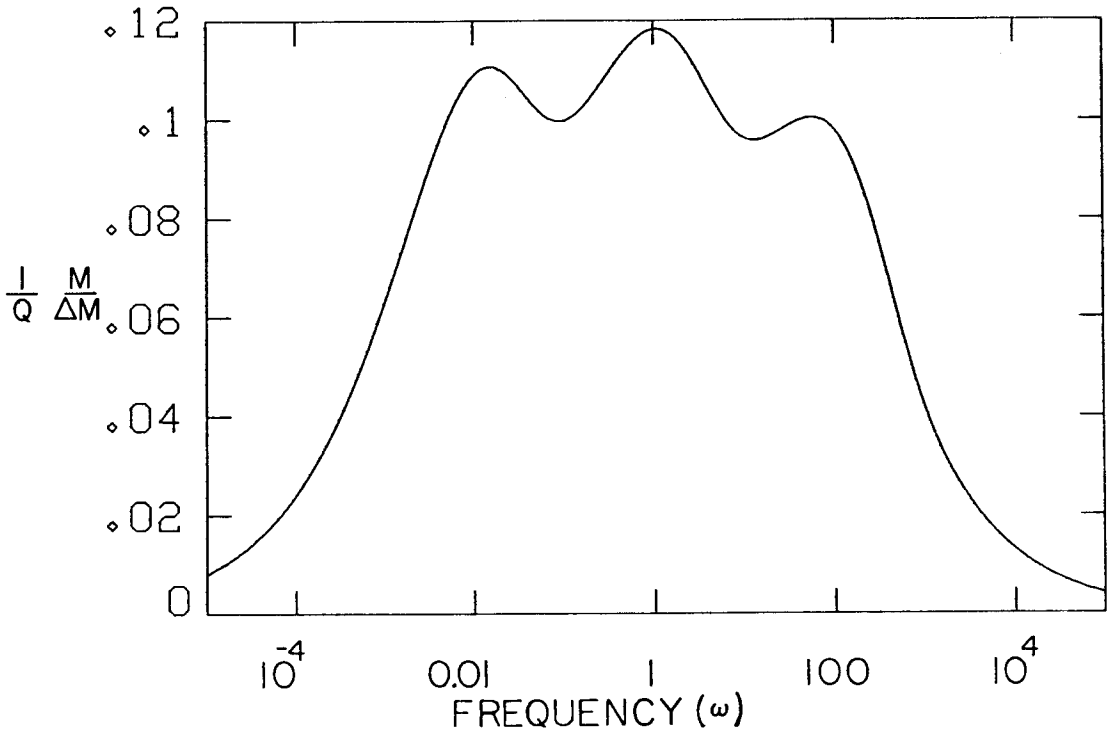

FIG. 5.3. Normalized attenuation, as a function of frequency for a rock where the pore space is equally divided between cracks with τ_1 equal to 0.1, 1 and 10 seconds. The value of r is unity.

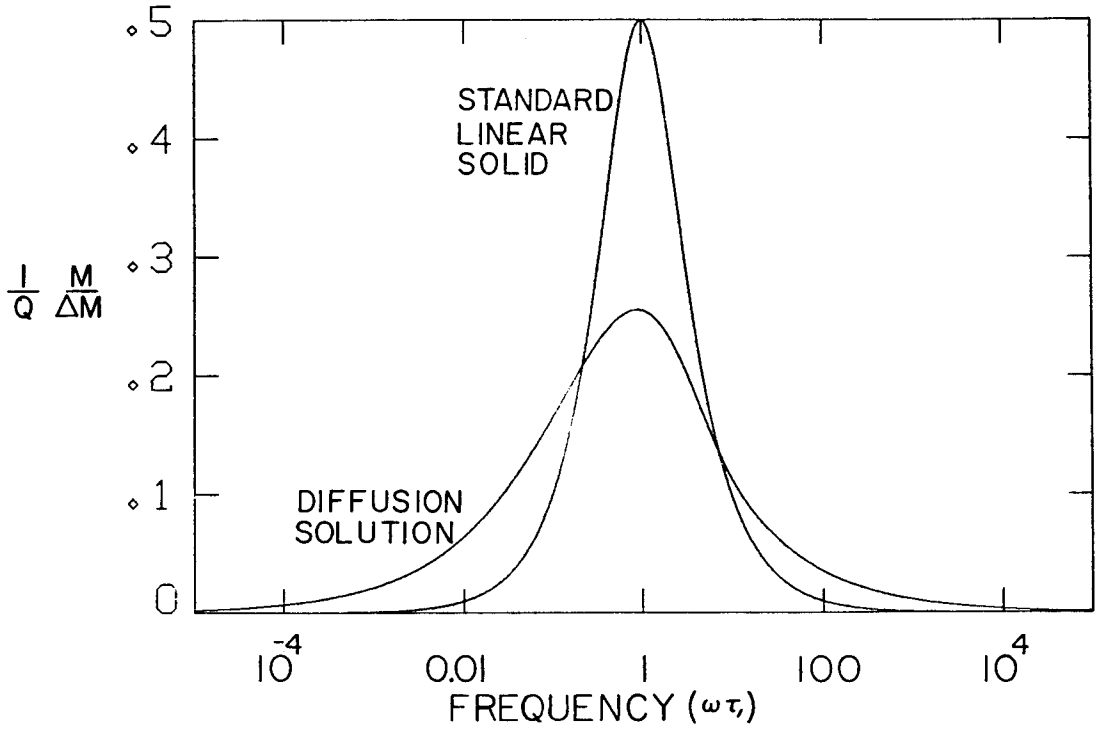

FIG. 5.4. Comparison between the standard linear solid and the diffusion solution.

	T ^oK	P Mpa	ρ $\frac{Kg}{m^3}$	$\alpha \cdot 10^6$ $^oK^{-1}$	K Pa	c $\frac{J}{^oKKg}$	h $\frac{J}{^oKms}$	b $\frac{^oK}{Pa}$	$\frac{K' - K}{K}$	D $\frac{mm^2}{s}$
limestone	300	300	2710	3.4	$76 \cdot 10^9$	840	3.85	$4.5 \cdot 10^{-10}$	$1.2 \cdot 10^{-4}$	1.7
quartzite	300	300	2640	1.1	$42 \cdot 10^9$	750	8.16	$1.6 \cdot 10^{-9}$	$7.1 \cdot 10^{-4}$	4.1
granite	300	100	2650	7.7	$46 \cdot 10^9$	590	-	$1.5 \cdot 10^{-9}$	$5.2 \cdot 10^{-4}$	-
water	293	0.1	990	202	$2.2 \cdot 10^9$	4190	0.6	$1.4 \cdot 10^{-8}$	$6.2 \cdot 10^{-3}$	0.14
water	554	10	773	2200	$5.5 \cdot 10^8$	5030	0.59	$3.2 \cdot 10^{-7}$	0.38	0.15
steam	373	0.1	0.6	2900	$1.0 \cdot 10^5$	2030	0.024	$9.0 \cdot 10^{-4}$	0.26	19
nitrogen	300	0.1	1.2	3330	$1.0 \cdot 10^5$	717	0.026	$1.2 \cdot 10^{-4}$	0.4	31

TABLE 5.2. Thermal properties of selected materials. Symbols are as defined in table 5.1. Thermodynamic data for rocks are from Simmons and Brace [1965] and Wong and Brace [1979]. Thermodynamic data for water and steam are obtained by differentiating the equation of state given by Keenan et al. [1969]. Thermodynamic parameters for nitrogen are those for a diatomic ideal gas. Conductivities for rocks are obtained by averaging values given by Clark [1966] for calcite and quartz. Conductivities for water, steam and nitrogen are from Weast [1964].

Magnitude estimation. The problem of determining the loss caused by any particular physical mechanism may be split into two parts, the estimation of the modulus defect, and the frequency dependence. It is often possible to estimate the modulus defect quite accurately, while a deterministic solution for the frequency dependence requires a detailed knowledge of the distribution and dimensions of the inhomogeneities responsible for the loss. In the remaining sections of this paper reversible thermodynamics will be used to estimate the modulus defect. A rough estimate of the range of frequencies involved may then be used to estimate the magnitude of the attenuation by a superposition of several loss peaks, as in figure 5.3. An alternative is to use the known general relationships between frequency dispersion and attenuation. For example, the assumption of a frequency-independent Q [Kjartansson, 1979] implies that

$$\frac{M(\omega)}{M(\omega_0)} = \left(\frac{\omega}{\omega_0}\right)^{2\gamma} \tag{5.27}$$

where

$$\frac{1}{Q} = \tan(\pi\gamma) \tag{5.28}$$

In the case where $Q \gg 1$, this may be rewritten:

$$\frac{M(\omega)-M(\omega_0)}{M(\omega_0)} = \frac{2}{\pi Q} \ln\left(\frac{\omega}{\omega_0}\right) \tag{5.29}$$

Thus a change in modulus when the attenuation is approximately independent of frequency over six orders of magnitude is related to 1/Q by

$$\frac{1}{Q} = \frac{\pi}{2 \ln\left[10^6\right]} \frac{\Delta M}{M} \approx \frac{1}{8} \frac{\Delta M}{M} \tag{5.30}$$

This result could also have been derived from figure 5.3.

The Magnitude of Thermoelastic Effects

In this section relations for the effective bulk modulus of rocks under various conditions will be developed and used to estimate the magnitude of loss due to thermoelastic effects. The high-frequency unrelaxed case is the simplest, as it implies periods too short for any thermal interactions to take place. Effects of porosity on the mechanical response of rocks have been treated by many authors. This includes both treatments where the pore space is assumed to be a distribution of elliptical inclusions or voids [Eshelby, 1957; Walsh, 1965; O'Connell and Budiansky, 1974], cracks of more general shapes [Mavko and Nur, 1978], or voids left between contacting spheres [Gassmann, 1951b; Mindlin and Deresewich, 1953]. These treatments all have it in common that the effective rock properties are derived from a detailed knowledge of the pore geometry as well as the intrinsic rock properties. Many of the models feature a strong dependence on poorly constrained parameters, for example aspect ratios.

In the present context we are interested in how the effective properties change as the response of the pore fluid changes, rather than in the absolute value of the effective moduli. A simple and elegant result derived by Gassmann [1951a] is ideally suited to this purpose. Gassmann's expression gives the effective bulk modulus in terms of the intrinsic bulk modulus of the rock matrix $\hat{K}$, the bulk modulus of the dry rock frame $\bar{K}$, the bulk modulus of the fluid $\tilde{K}$, and the porosity ϕ:

$$K = \frac{\hat{K}(\bar{K}+R)}{\hat{K}+R} \tag{5.31}$$

where

$$R = \frac{\tilde{K}(\hat{K}-\bar{K})}{\phi(\hat{K}-\tilde{K})} \tag{5.32}$$

The pore geometry enters into this expression only through its effect on the frame modulus ($\bar{K}$) and the porosity. Both parameters can be measured directly, as well as the intrinsic moduli of the pore fluid and the rock matrix.

In our use of Gassmann's relations, two assumptions are implicit. We will assume that the rock matrix has a zero thermal expansivity. As shown in table 5.2, the thermal expansivity of the rocks is at least an order of magnitude less than the thermal expansivity of the fluids, except for water at temperatures near 4°C. Attenuation due to thermal effects is so small when the rock and fluid have comparable thermal expansivities, that it will probably be masked by other mechanisms, such as viscous dissipation. When the expansivities are greatly different, however, attenuation may be substantial.

Shear effects. Equation (5.31) gives only relations for the bulk modulus, and is derived on the assumption that the rock is isotropic on a macroscopic scale and that the pore-fluid pressure is uniform throughout the pore volume. This implies that all the pores are connected and neglects the viscosity of the pore fluid. These assumptions are probably quite good for rocks where well-connected round pores are dominant. Gassmann's theory has been used successfully in the interpretation of seismic data for sedimentary materials [Brown and Korringa, 1975].

Winkler [1979] found that both the shear velocity and the attenuation in a porous Vycor glass are much less sensitive to changes in the pore fluid than compressional velocity and attenuation. In contrast, experiments with granite samples showed significant dependence of both shear and compressional properties on the state of the pore contents. For a rock that contains an isotropic random distribution of ***isolated*** flat cracks, both shear and bulk moduli will depend on the bulk modulus of the pore fluid [Korringa et al., 1979]. Mavko and Nur [1979] have estimated that the effects of the pore fluids on the shear response in rocks containing flat crack may be about half the effect on compressional deformations.

Estimation of effective bulk moduli. We seek expressions for the adiabatic bulk modulus of pore fluids under various conditions. We have chosen to express the results in terms of parameters that may be measured under conditions of either constant pressure or temperature. Thus we will express the adiabatic bulk modulus K' and the rate of temperature increase with pressure b in terms of the isothermal bulk modulus K, the density ρ or the specific volume V, the heat capacity at constant pressure c, and the coefficient of thermal expansivity α. The parameters are defined in table 5.1.

One of Maxwell's relations [Kelly, 1973, p. 142] enables us to write the stress heating coefficient, b, as

$$b = \left(\frac{\partial T}{\partial P}\right)_S = \left(\frac{\partial V}{\partial S}\right)_P \tag{5.33}$$

In the absence of any phase transitions this becomes

$$b = \frac{\left(\frac{\partial V}{\partial T}\right)_P}{\left(\frac{\partial S}{\partial T}\right)_P} = \frac{T\alpha V}{c} = \frac{T\alpha}{\rho c} \tag{5.34}$$

In order to get the adiabatic bulk modulus K' we may write

$$\left(\frac{\partial V}{\partial P}\right)_S = \left(\frac{\partial V}{\partial P}\right)_T + \left(\frac{\partial V}{\partial T}\right)_P \left(\frac{\partial T}{\partial P}\right)_S \tag{5.35}$$

Using the definitions in table 5.1, this reduces to

$$\frac{1}{K'} = \frac{1}{K} - \alpha b \tag{5.36}$$

Equations (5.34) and (5.36) may be applied to heterogeneous systems, as long as no phase transitions take place. The isothermal bulk modulus and the isobaric expansivity and heat capacity are not defined in the presence of phase transitions: this case will be treated separately. The parameters used will now be the effective parameters, K_e, α_e, c_e and V_e, for the system that is being analyzed. For a porous rock where the matrix has no thermal expansivity, a specific volume V_r, heat capacity c_r, and porosity ϕ, and a pore space containing a mixture of two fluids, indicated by subscripts 1 and 2 where the mass fraction of the first fluid is x, we have the following relations for the effective parameters of the pore mixture:

$$V_e = xV_1 + (1-x)V_2 \tag{5.37}$$

$$\frac{1}{K_e} = \frac{1}{V_e}\left[\frac{xV_1}{K_1} + \frac{(1-x)V_2}{K_2}\right] \tag{5.38}$$

$$\alpha_e = \frac{1}{V_e}\left[xV_1\alpha_1 + (1-x)V_2\alpha_2\right] \tag{5.39}$$

$$c_e = xc_1 + (1-x)c_2 + \frac{V_e(1-\phi)c_r}{V_r\phi} \tag{5.40}$$

Water-saturated rock. We will first consider a rock saturated with liquid water. In this case $x = 1$, $V_e = V_1$, $K_e = K_1$, $\alpha_e = \alpha_1$ and

$$c_e = c_1 + \frac{V_1}{V_r}\frac{1-\phi}{\phi}c_r \tag{5.41}$$

Thus the only difference between the unrelaxed high-frequency limits, where there is no thermal interaction, and the fully relaxed limit, is an increase in the effective heat capacity of the liquid; the rock matrix acts as a heat sink. The second term in equation (5.41) will tend to dominate when $\phi \ll 1$. For low-porosity rocks the relaxed case is well-approximated by using the isothermal bulk modulus for the fluid.

Keenan et al. [1969] give an empirical equation of state that fits the observed behavior of liquid water and steam at pressures less than 100 Mpa (1000 bar) and at temperatures less than 1000°C. Differentiation of this equation yields an internally consistent set of thermodynamic parameters for water and steam. Figure 5.5 shows a plot of the isothermal and adiabatic bulk moduli of water, as functions of temperature, at the boiling pressure. At room temperature there is little difference between the two curves, but the difference increases rapidly at higher temperatures. Another noteworthy feature on this plot is the rapid decrease of both the isothermal and adiabatic bulk moduli at temperatures above 100°C.

Figure 5.6 shows P-wave velocities for three different rocks as functions of temperature at a pore pressure of 10 Mpa (100 bar). The rocks have the same intrinsic matrix velocity (6.5 km/s) and the same dry P-velocity (1.5 km/s), with Poisson ratios of .25 and .2, respectively. Porosities were chosen so as to give saturated velocities of 2, 3, and 4 km/s. Two curves are shown for each rock, one for the unrelaxed case and one for the relaxed case.

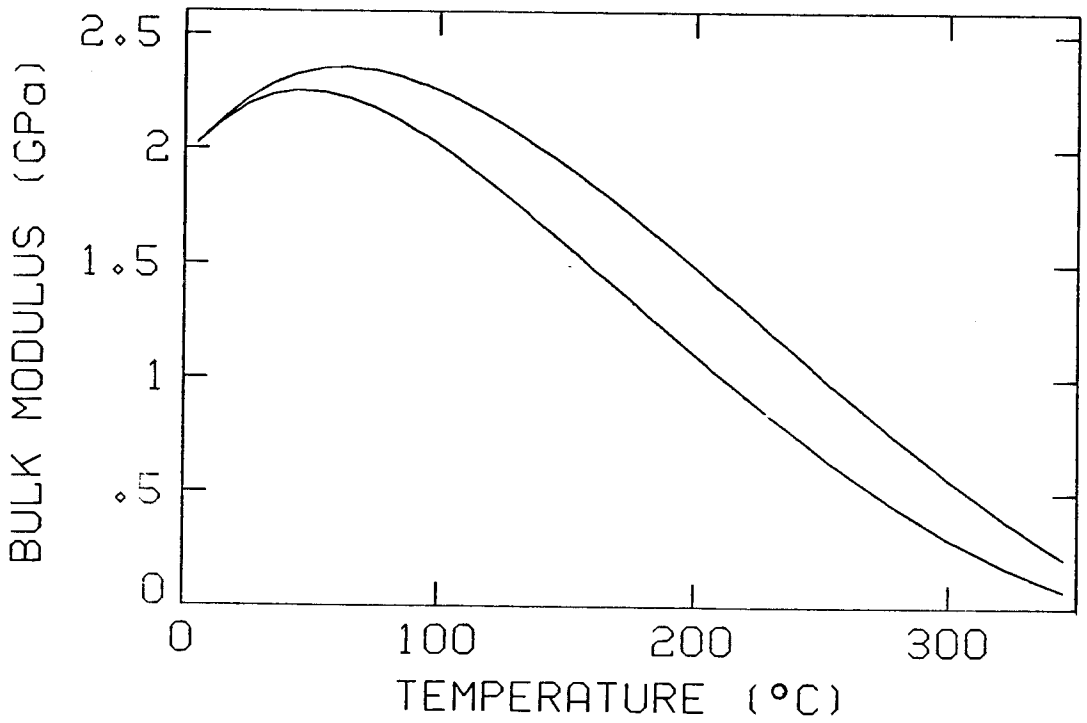

FIG. 5.5. Adiabatic and isothermal bulk moduli of water, as functions of temperature, at boiling pressure.

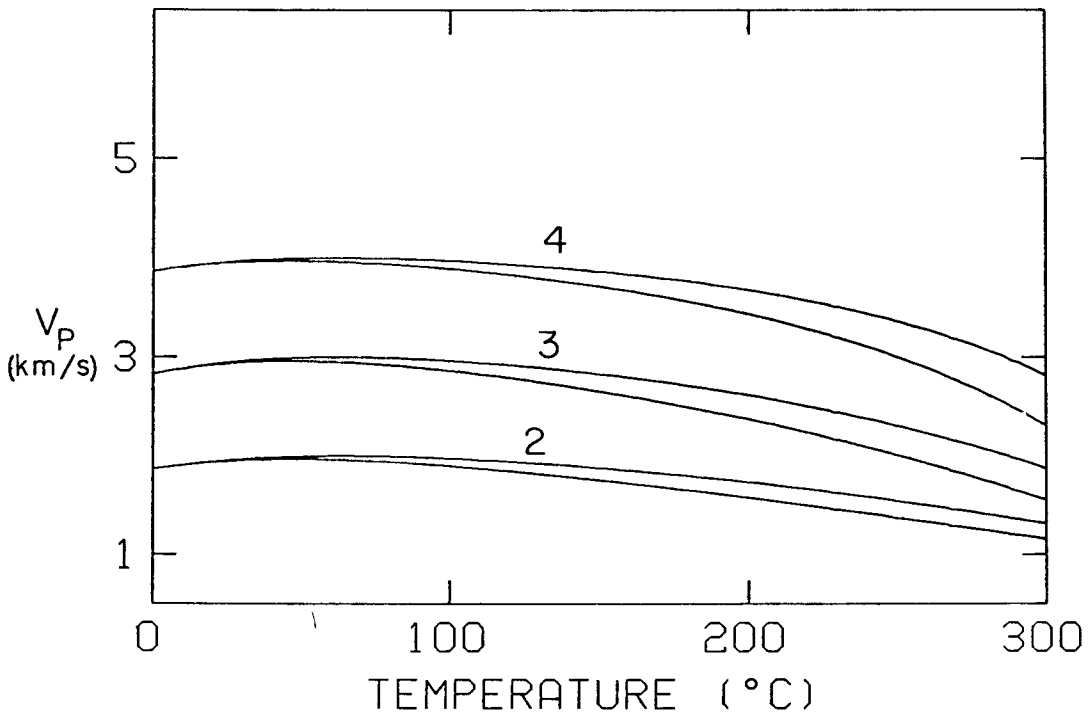

FIG. 5.6. P-wave velocities for three different rocks saturated with liquid water, plotted vs. temperature. The upper curve in each pair is the unrelaxed, the lower is the relaxed velocity. The three rocks have the same dry velocity, 1 km/s, and the same matrix material with a P-velocity of 6.5 km/s. Porosities were chosen to give maximum saturated velocities of 2, 3 and 4 km/s. Pore pressure is 10 MPa.

Figure 5.7 shows the attenuation obtained by applying equation (5.30) to the results from figure 5.6. All three curves show a strong increase in attenuation with temperature. The example with the lowest porosity and the highest saturated velocity shows stronger temperature dependence than the other; this is due to an increase in the fraction of the total strain energy that is stored in the pore fluid as its compressibility increases.

The examples in figures 5.6 and 5.7 were computed for specified values of the dry and saturated velocities. For comparison with *in-situ* observations, it may sometimes be more desirable to specify porosity rather than dry velocity since the latter may be more readily estimated. Figure 5.8 shows a contour plot of the attenuation, predicted as a function of porosity and temperature, for a rock with a saturated velocity of 4 km/s and an intrinsic velocity of 6.5 km/s. As before, a strong dependence of attenuation on temperature is indicated, but at high temperatures the attenuation increases as porosity (and the dry velocity) decreases.

Gas and liquid. The second example that we will consider is for rock where the pore space contains a mixture of a gas phase and liquid water, such that the two materials do not interact except through the flow of heat from one to the other. Figure 5.9 shows relaxed and unrelaxed velocities for three different rocks, chosen to have properties similar to those used by Domenico [1974], as representative of sand reservoir rocks at depths of 600, 1800 and 3000 meters (2000, 6000, and 10000 feet). The corresponding attenuation values are plotted in figure 5.10. The gas is assumed to be an ideal gas with the ratio between the adiabatic and isothermal bulk moduli $\gamma = 1.4$, the theoretical value for a diatomic gas. The density was assumed to be that of air, $a = 0.029 kg/mol$. The other parameters are given by

$$V = \frac{RT}{aP} \tag{5.42}$$

$$K = P \tag{5.43}$$

$$\alpha = \frac{1}{T} \tag{5.44}$$

$$c = \frac{R}{(\gamma-1)a} \tag{5.45}$$

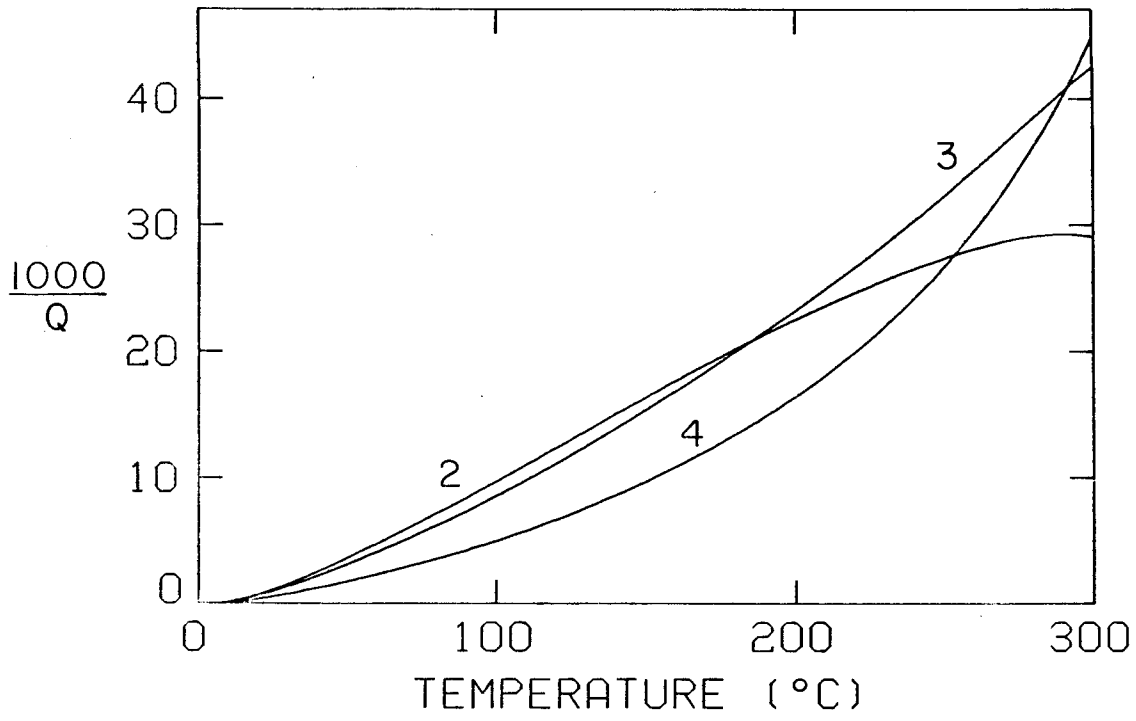

FIG. 5.7. Attenuation as a function of temperature for the conditions in figure 5.6.

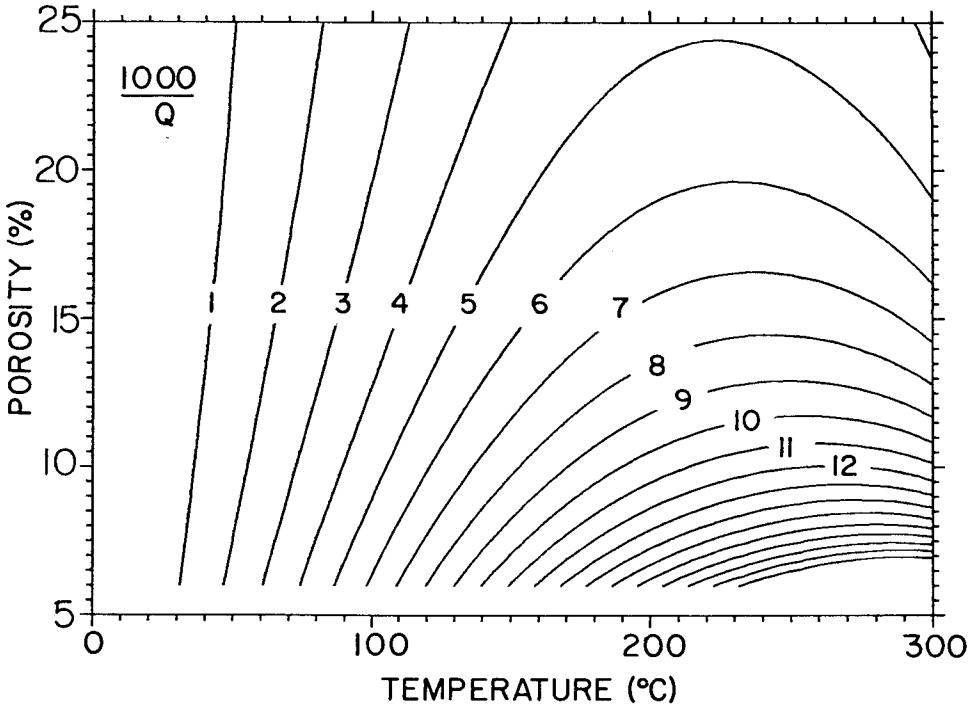

FIG. 5.8. Attenuation for water-saturated rocks, as a function of temperature and porosity, for rocks with a P-wave velocity of 3.5 km/s at 65°C and an intrinsic matrix velocity of 6.5 km/s.

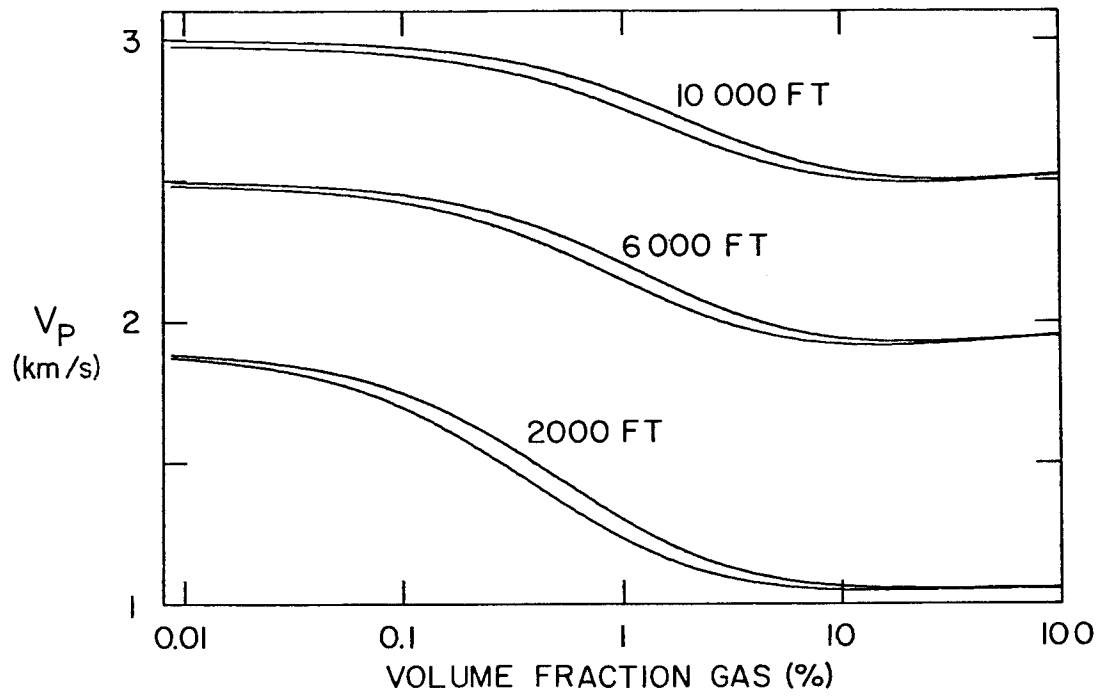

FIG. 5.9. Computed relaxed and unrelaxed P-wave velocities for rocks containing a mixture of gas and water. Rock parameters are the same as used by Domenico [1974], as representative of conditions in sand reservoirs at depths of 2000, 6000 and 10,000 feet.

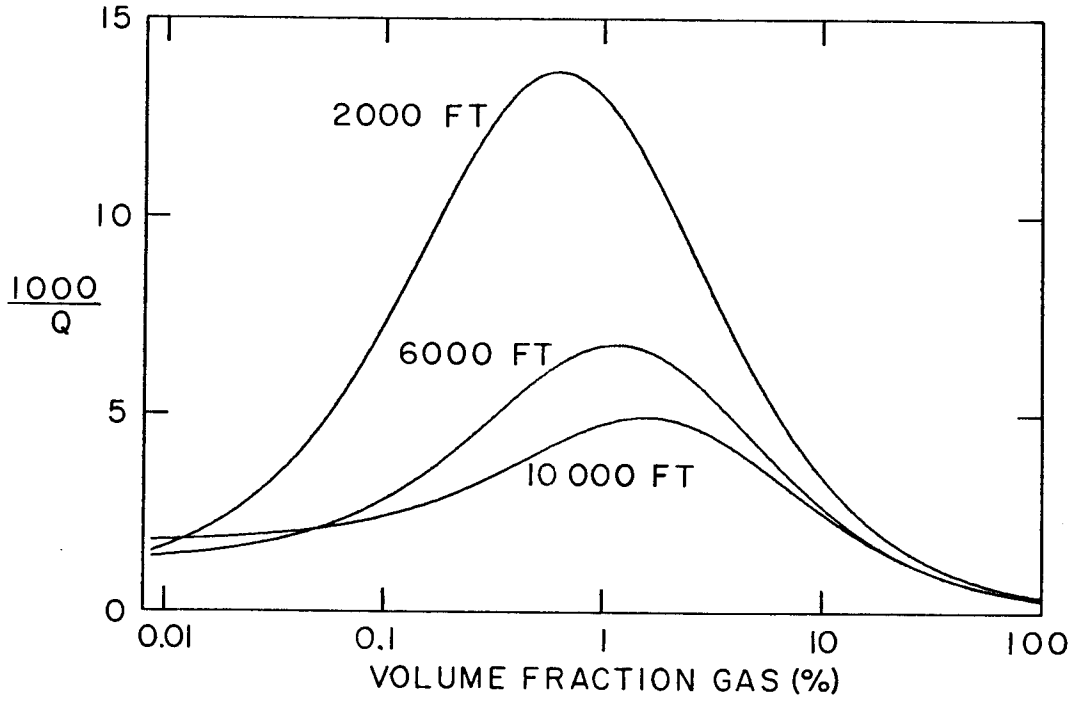

FIG. 5.10. Attenuation for the rocks in figure 5.9.

where R is the gas constant, 8.314 J/mol. The gas parameters are combined with those for water using equations (5.37)-(5.40) and then substituted into Gassmann's formula (5.31).

Our results show the same qualitative dependence of velocity on gas saturation as was reported by Domenico [1974], while there is a substantial drop in velocity as small amounts of gas are introduced into water-saturated rock; there is little difference in velocity between rocks with 10% and 100% of the pore volume gas, for all of the cases shown. Attenuation increases as gas is introduced into the pore space, reaches a peak, and then falls off and is minimum when no water is left in the pores. The gas saturation at the peak is roughly proportional to the pore pressure. The examples in figure 5.10 show a large change in attenuation as the gas fraction changes from 5% to 100%, while the velocity is virtually unchanged over this range. This may be of interest in exploration for natural gas and geothermal resources.

Winkler and Nur [1979] and Frisillo and Stewart [1979] present laboratory results showing the same qualitative features, but with the attenuation peak occurring when the gas saturation is between 10% and 30%. This discrepancy between our theoretical and these experimental results may be caused by microscopic inhomogeneities in the pore space. The pore space may consist of both wide pores and relatively flat cracks, which are not all connected at the sonic and ultrasonic frequencies used in these experiments.

Systems with more than one phase. In the presence of phase transitions we can no longer use equation (5.35) since $(\partial V/\partial P)_T$ is not finite. To get the effective adiabatic bulk modulus we may write

$$\left(\frac{\partial V}{\partial P}\right)_S = \left(\frac{\partial V}{\partial T}\right)_S \left(\frac{\partial T}{\partial P}\right)_S \tag{5.46}$$

Use of the Maxwell's relation (5.33) yields the Clausius-Clapeyron equation

$$b = \frac{dT}{dP} = \frac{T(V_1 - V_2)}{L_{12}} \tag{5.47}$$

where L_{12} is the latent heat released in the transition from state 1 to state 2. The other factor on the left side of (5.46) is obtained by writing

$$\left(\frac{\partial V}{\partial T}\right)_S = \left(\frac{\partial V}{\partial T}\right)_{P,x} + \left(\frac{\partial V}{\partial P}\right)_{T,x}\left(\frac{\partial P}{\partial T}\right)_S + \left(\frac{\partial V}{\partial X}\right)_{P,T}\left(\frac{\partial X}{\partial T}\right)_S \qquad (5.48)$$

The first term in (5.48) is obtained from equations (5.39) and the second term from (5.38) and (5.47). For the final term we have

$$\left(\frac{\partial V}{\partial X}\right)_{P,T} = (V_2 - V_1) \qquad (5.49)$$

The final factor, $(\partial X/\partial T)_S$, is obtained by writing

$$\left(\frac{\partial S}{\partial T}\right)_S = 0 = \left(\frac{\partial S}{\partial X}\right)_{P,T}\left(\frac{\partial X}{\partial T}\right)_S + \left(\frac{\partial S}{\partial T}\right)_{P,x} + \left(\frac{\partial S}{\partial P}\right)\left(\frac{\partial P}{\partial T}\right)_S \qquad (5.50)$$

Through the use of Maxwell's fourth relation [Kelly, 1973], this becomes

$$\left(\frac{\partial X}{\partial T}\right)_S = \frac{-\left(\frac{\partial S}{\partial T}\right)_{P,x} + \left(\frac{\partial V}{\partial T}\right)_{P,x}\left(\frac{\partial P}{\partial T}\right)_S}{\left(\frac{\partial S}{\partial X}\right)_{P,T}} \qquad (5.51)$$

Substitution of equations (5.48) and (5.51) into (5.46) and the definition of the bulk modulus give the result

$$\frac{1}{K'} = \frac{1}{K_e} - 2b\alpha_e + \frac{b^2 c_e}{V_e T} \qquad (5.52)$$

where b is given by equation (5.47) and V_e, α_e, and c_e are given by equations (5.37), (5.39), and (5.40).

We have applied equation (5.52) to two cases. One is a porous rock where the pore space contains a mixture of water and steam. The relaxed and unrelaxed velocities are shown as functions of mass fraction steam in figure 5.11. Figure 5.12 shows the corresponding attenuation. The introduction of any steam into a water-saturated rock results in a drop of the effective relaxed modulus, to a value that is essentially the same as the modulus of the dry rock. This results in attenuation that is much greater than when phase transitions are absent.

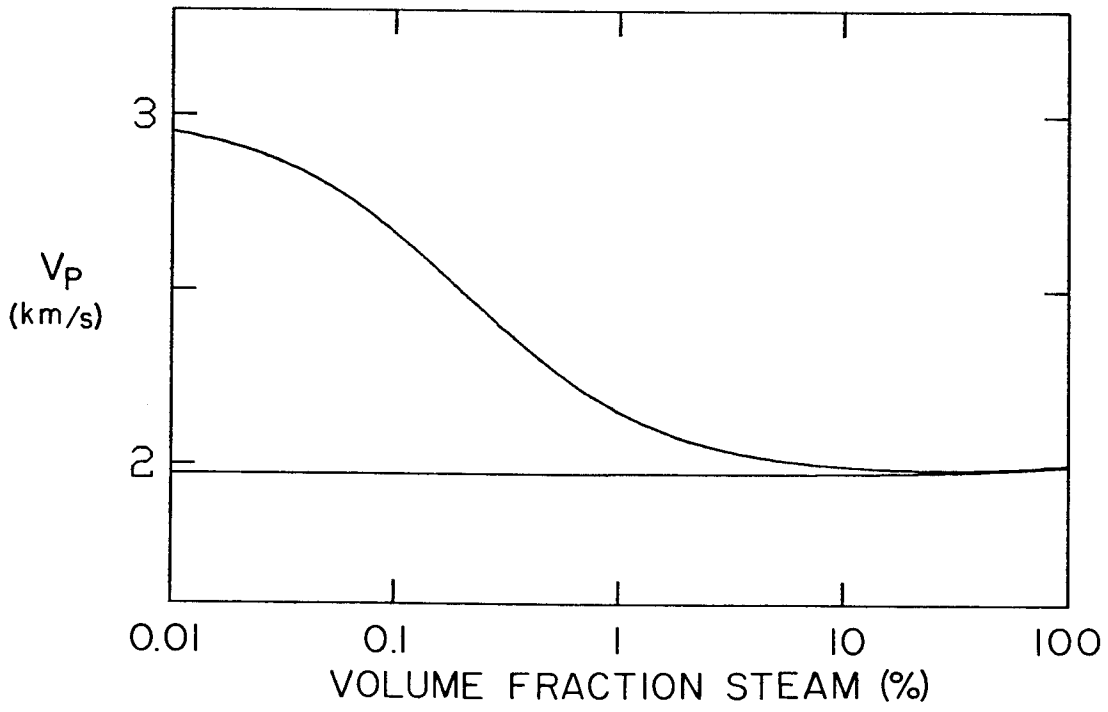

FIG. 5.11. Relaxed and unrelaxed P-wave velocities for a rock containing a mixture of water and steam at a temperature of 200°C. The dry velocity is 2 km/s and the saturated velocity is 3 km/s.

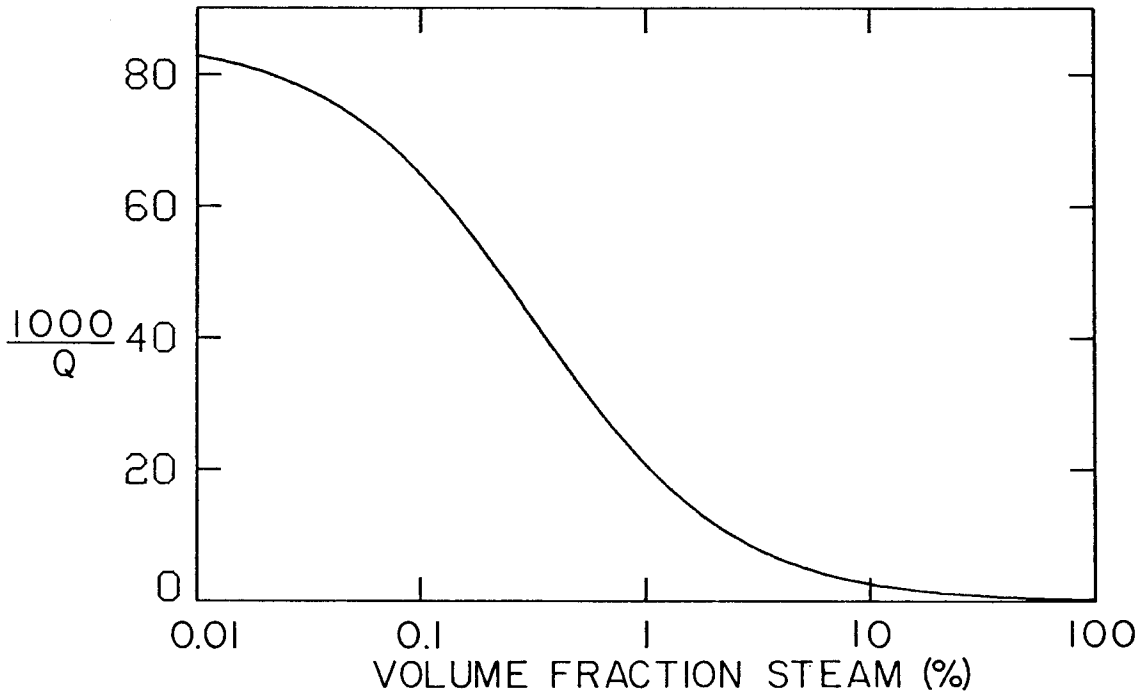

FIG. 5.12. Attenuation for the conditions in figure 5.11.

Another case where phase transitions are expected to play a significant role is in rocks that contain partial melt. Carmichael et al. [1977] give equations of state for several minerals that satisfy measured heat capacities and the observed dependence of melting temperature on pressure up to about 4 GPa (40 kbar). They give empirical relations for (1) the dependence of the specific volume on both temperature and pressure, and (2) heat capacity and the latent heat of fusion at room pressure. The empirical expressions are readily integrated to obtain the Gibbs free energy as a function of temperature and pressure. The Gibbs free energy may be used to compute the melting temperature, and differentiated to yield the heat capacity at any pressure. The resulting set of thermodynamic parameters is guaranteed to be internally consistent; this is important because equations (5.36) and (5.52) involve differences between terms of similar size. Figure 5.13 shows the effective bulk modulus for a mixture of solid and liquid olivine (fayalite), for three different cases: unrelaxed without any phase transitions or heat flow; thermal equilibrium without any phase transitions, and both thermal and phase equilibria. Figure 5.14 shows the attenuation, both with and without phase transitions. In these examples we have neglected the effects of the shear strength of the solid phase. The effect of the shear strength of the rock is to reduce the difference between the relaxed and unrelaxed effective moduli, and thus the attenuation at low melt fractions, unless the melt surrounds the solid grains or is in the form of very thin films. The effects of other melt configurations are treated in detail by Mavko [1979].

Implications for Exploration

Hydrocarbons. Most of the cases where we have predicted significant absorption due to thermal effects are of interest in the exploration for energy resources. The calculations for water and gas mixtures should give an indication of the degree of losses that might be expected in rocks that contain gas. Our results for this case, as shown in figure 5.10, indicate that thermal relaxation will be responsible for a significant amount of absorption when gas is present in small amounts, and that the loss will be strongly dependent on the degree of gas saturation, even in the range where the wave velocities are insensitive to the amount of gas present. The results from figure 5.10 would have been virtually the same had an incompressible liquid

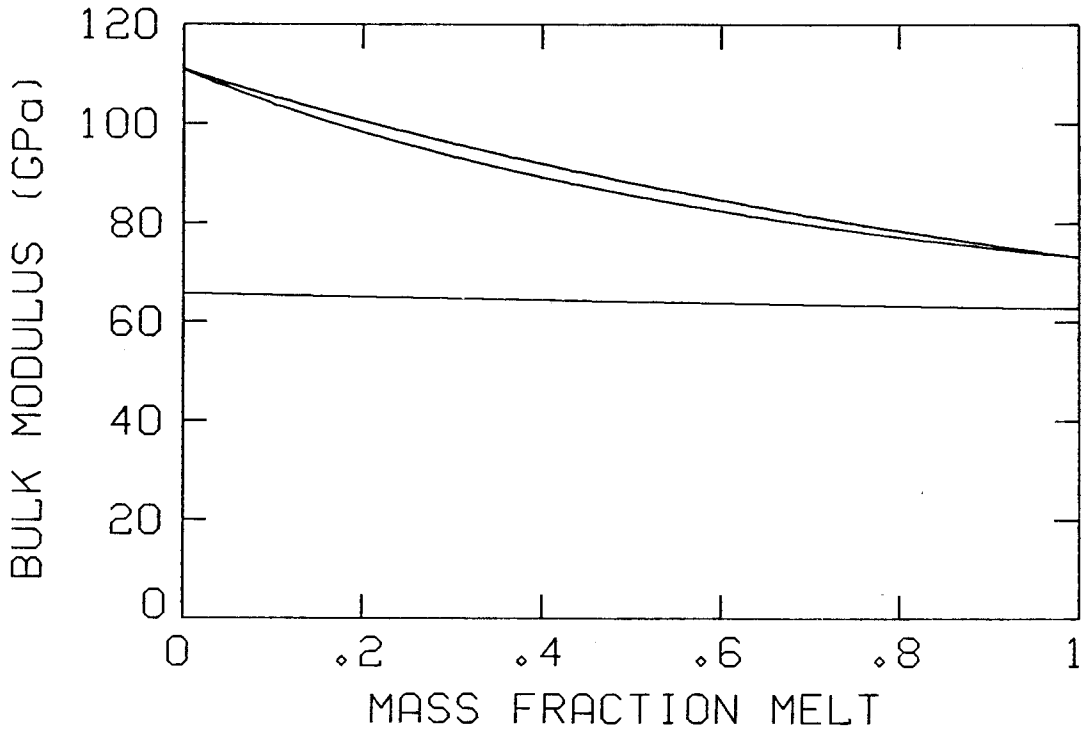

FIG. 5.13. Bulk modulus of olivine as a function of massfraction melt, at a pressure of 2 GPa. Shown are the unrelaxed bulk modulus (top curve), the thermally relaxed without phase transitions, and the completely relaxed bulk modulus including the effects of phase transitions (bottom).

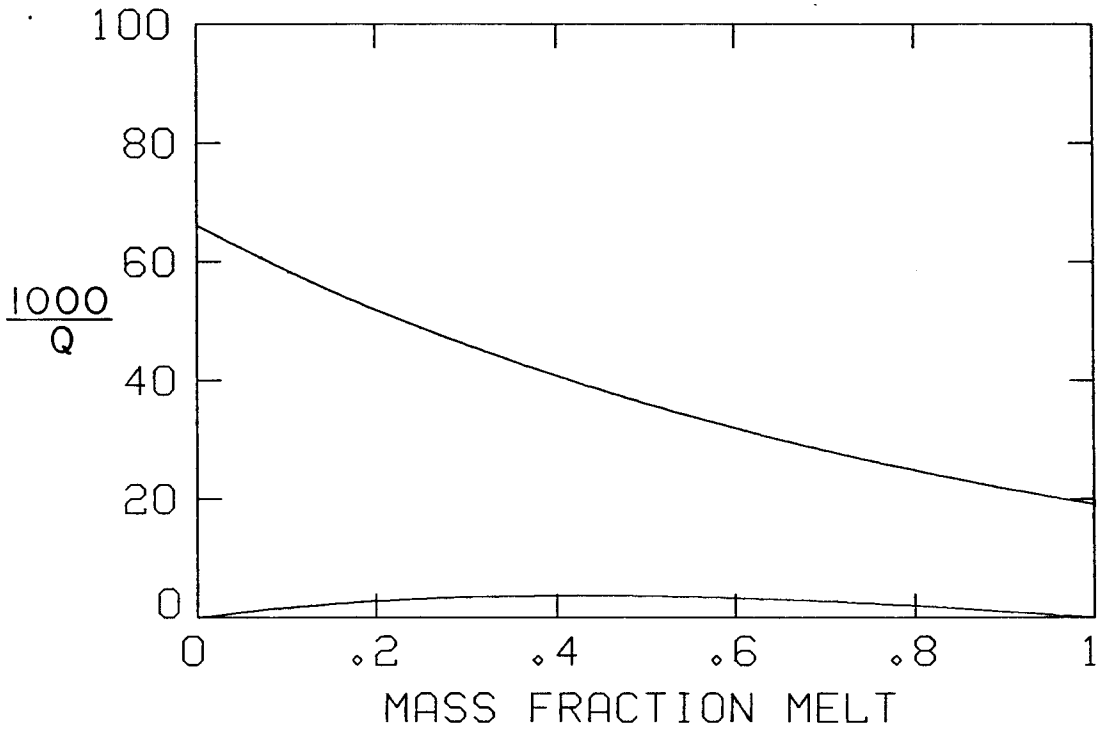

FIG. 5.14. Attenuation for olivine under the same conditions as in figure 5.13. Upper curve is the attenuation when phase transitions are included; the lower curve shows the attenuation caused by heat flow without any phase transitions.

been used instead of water; the loss is controlled primarily by the properties of the gas. As most gases have properties similar to ideal gas, the results from figure 5.10 do apply to any gas-liquid mixtures, as long as the gas does not dissolve in the liquid. Any solubility of the gas in the liquid will have the effect of lowering the relaxed bulk modulus and thus increasing the absorption. This may be the case in most, if not all cases involving hydrocarbons *in situ*, whether the fluid is brine or oil. Consequently, the calculations in figure 5.10 should be considered lower bounds for the absorption due to thermal relaxation. The actual response of oil-gas or brine-gas mixtures may be more like the response of water-steam mixtures (figure 5.12).

It has been noted in the literature that anomalously low amplitudes are sometimes associated with gas zones [Sheriff, 1975; Dobrin, 1976].

Geothermal. Several of the conditions that result in significant thermal losses are related to features of interest in geothermal exploration. Some of the larger concentrations of geothermal energy are associated with recent igneous activity. Observations of P-wave absorption may aid in the location of zones of partial melt at depth, and thus delineate potential sources of heat.

Geothermal energy is utilized in three different forms, each of which is presently of roughly the same economic significance. Low-temperature thermal waters, with temperature at depth ranging from 65^{o}C to 200^{o}C, are useful as a direct source of heat for space heating and various industrial processes. If the pore pressure at depth is anywhere close to hydrostatic, the water will be in the liquid state and boiling will only take place very near the surface. The results from figures 5.6-5.8 are relevant to those circumstances, and imply that the absorption will increase almost linearly with temperature, at temperatures from 50^{o}C to 200^{o}C.

The results of our calculations for liquid water are also applicable to high-temperature geothermal systems. Figure 5.15 shows the boiling temperature of water, as a function of pore pressure. Boiling temperature of 180^{o} is reached at a depth of about 100 m, if the pore pressure is hydrostatic. At higher temperatures the boiling point curve does level off toward the critical point at 374^{o}C and a pressure of 22.1 MPa. It is thus possible that high-temperature water-dominated systems could reach the boiling pressure at depth, even if the pore pressures are close to hydrostatic. This would result

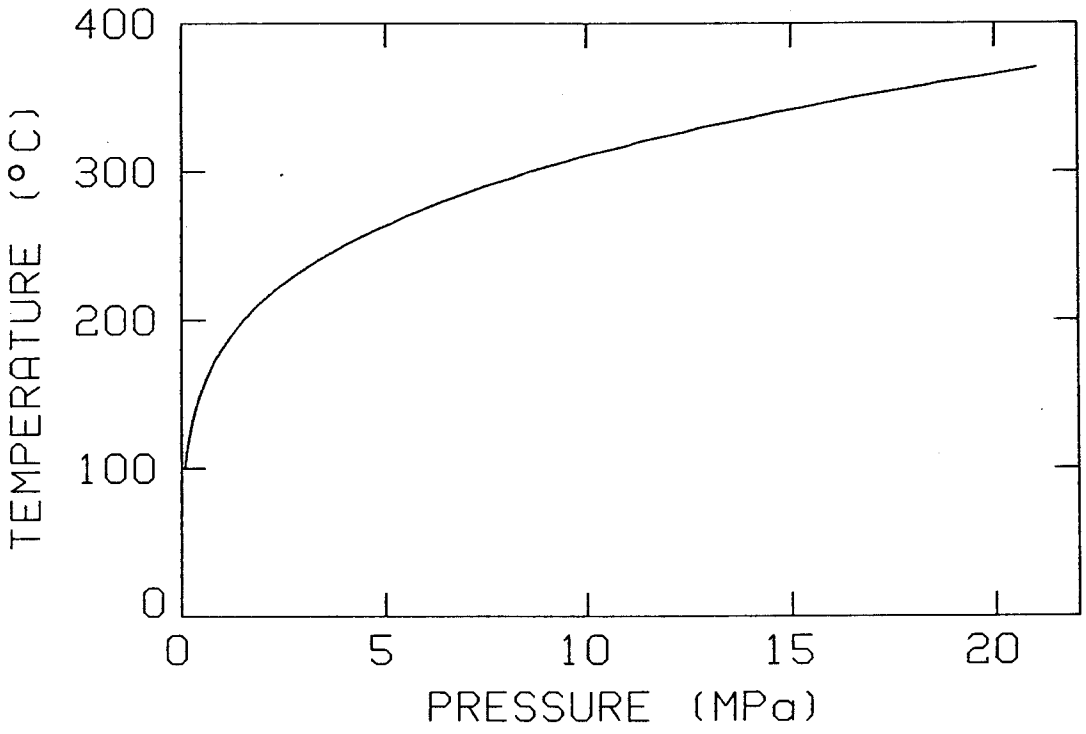

FIG. 5.15. Boiling temperatures of water as a function of pressure.